Chinese Physics Letters

LETTER

Multipartite Controlled-NOT Gates Using Molecules and Rydberg Atoms

Cite as: Yi-Han Bai *et al*. 2026 *Chin. Phys. Lett.* **43** 080302

DOI CSTR

Recommended Articles

Nonadiabatic Holonomic Quantum Computation Based on Rydberg Ground State Blockade
Shi-Lei Su, Chen Wang, P.-Y. Song, and Gang Chen
Chin. Phys. Lett. **41**, (2024)

Analysis of Heralded Higher-Fidelity Two-Qubit Entangling Gates with Self-Correction
Yuan Sun
Chin. Phys. Lett. **42**, 070602 (2025)

Quantum Simulation of Two-Dimensional U(1) Gauge Theory in Rydberg and Rydberg-Dressed Atom Arrays
Zheng Zhou, Zheng Yan, Changle Liu, Yan Chen, and Xue-Feng Zhang
Chin. Phys. Lett. **42**, 053705 (2025)

Vortex Dynamics in Binary Ultracold Rydberg Atomic System
Yu Zhong, Dan-Feng Yang, Ya-Xian Liu, Jia Li, Houria Triki, and Qin Zhou
Chin. Phys. Lett. **42**, 080002 (2025)

High-Fidelity Two-Qubit Quantum Logic Gates in a Trapped-Ion Chain Using Axial Motional Modes
Xingyu Zhao, Ji Bian, Yi Li, Yue Li, Mengxiang Zhang, and Yiheng Lin
Chin. Phys. Lett. **42**, 110601 (2025)

Cavity-Enhanced Rydberg Atom Microwave Receiver
Bang Liu *et al*.
Chin. Phys. Lett. **42**, 053201 (2025)

A series journal of Chinese Physical Society distributed by IOP Publishing

Chinese Physics Letters

Chin. Phys. Lett. **43** 080302 (2026)

LETTER

DOI: 10.1088/0256-307X/43/8/080302
CSTR: 32039.14.0256-307X.43.8.080302

Multipartite Controlled-NOT Gates Using Molecules and Rydberg Atoms

Yi-Han Bai(柏艺涵)[1,†], Yue Wei(魏越)[1,†], Chi Zhang(张驰)[2], Weibin Li(李伟斌)[3,*], and Xiao-Qiang Shao(邵晓强)[1,4,*]

[1]Center for Quantum Science and School of Physics, Northeast Normal University, Changchun 130024, China
[2]Centre for Cold Matter, Blackett Laboratory, Imperial College London, Prince Consort Road, London SW7 2AZ, United Kingdom
[3]School of Physics and Astronomy, and Centre for the Mathematics and Theoretical Physics of Quantum Non-equilibrium Systems, The University of Nottingham, Nottingham NG7 2RD, United Kingdom
[4]Institute of Quantum Science and Technology, Yanbian University, Yanji 133002, China

[†]These authors contributed equally to this work.
[*]Corresponding authors. Email: weibin.li@nottingham.ac.uk; xqshao@nenu.edu.cn

Multi-qubit quantum gates offer an efficient pathway to reducing circuit depth in quantum information processing. Here, we propose two multipartite controlled-NOT gate schemes in a hybrid platform composed of polar molecules and Rydberg atoms. By encoding the control qubits in the long-lived ground states of polar molecules and harnessing the strong dipole–dipole interactions of Rydberg atoms, our approach establishes a gate mechanism that enables both strong and controllable coupling while effectively suppressing decoherence. The scheme can be naturally generalized to larger systems, providing a scalable route toward hybrid quantum computation.

Quantum computing holds the potential to tackle problems beyond the reach of classical approaches [1−4]. Universal quantum computation can be realized using single- and two-qubit operations [5,6]. Such decompositions, though general, often result in deep circuits and significant resource overhead in large-scale settings. Multi-qubit gates offer a more direct strategy for reducing circuit depth and enhancing operational efficiency, making them indispensable for scalable quantum information processing [7−13]. Achieving fast, high-fidelity, and scalable implementations remains challenging, largely constrained by finite coherence times and the rapidly growing complexity of control in larger systems. Hybrid quantum systems present a viable route to address these issues by integrating the distinct advantages of different platforms [14−16]. In these architectures, roles can be allocated across subsystems, which helps minimize crosstalk and suppress decoherence. Within this context, hybrid quantum gates are typically grouped into two classes: direct-coupling approaches, based on intrinsic interactions between subsystems, and mediated approaches, where effective interactions are established through an auxiliary system [17−21].

Neutral atoms confined in optical tweezer arrays constitute a versatile platform for quantum information processing, owing to their high reconfigurability and flexible qubit connectivity [22−25]. Excitation to Rydberg states further extends their capabilities by providing long-lived excited states, along with strong and tunable dipole–dipole or van der Waals interactions [26−30]. Compared with single-species neutral-atom platforms, heteronuclear Rydberg architectures have recently emerged as a promising route toward scalable quantum information processing [31,32]. The distinct optical transition frequencies of different atomic species enable intrinsically species-selective addressing with negligible crosstalk, while asymmetric interactions engineered via Förster resonances can effectively suppress the interaction between the target atoms during parallel gate operations. These features make multi-species atomic systems particularly well suited for the implementation of complex quantum logic. Building on this concept, hybrid molecule–Rydberg-atom platforms further enrich the multi-species paradigm by harnessing the complementary strengths of polar molecules and Rydberg atoms [33]. Polar molecules offer rich internal state structures, long coherence times, and permanent electric dipole moments in their rotational ground states [34−37], thus enabling strong and controllable conditional interactions with nearby Rydberg atoms. Indeed, recent experiments and theoretical proposals have demonstrated fast, high-fidelity molecular quantum gates mediated by Rydberg interactions [38−41]. Moreover, owing to the enormous frequency separation between molecular microwave transitions (GHz) and atomic optical transitions (THz), hybrid molecule–Rydberg-atom systems provide an even higher degree of spectral isolation than heteronuclear atomic platforms, substantially mitigating control crosstalk. Despite these advances, existing studies have focused primarily on two-qubit operations. The realization of efficient multi-qubit controlled-NOT (CNOT) gates that fully leverage the unique capabilities of hybrid molecule–Rydberg-atom architectures remains an important outstanding challenge.

In this work, we propose two multipartite CNOT gate schemes in a hybrid molecule–Rydberg-atom platform, featuring two-control and two-target configurations. The approach relies on direct dipole–dipole interactions between polar molecules and Rydberg atoms. The control qubits are encoded in the electronic ground states of molecules, enabling stable trapping and reduced motional decoherence, while Rydberg excitations provide strong and tunable interactions to realize fast, high-fidelity gate operations. Numerical simulations demonstrate high-fidelity performance, with only slight degradation arising from Rydberg-state decay. Furthermore, the scheme is extended to a four-qubit gate, confirming its feasibility and indicating a clear path toward generalization to larger multi-qubit systems.

As shown in Fig. 1(a), we consider two CaF molecular control qubits and one ^{87}Rb atomic target qubit arranged in a symmetric geometry, with the atom located equidistantly from the two molecules. Although this symmetric configuration is adopted for clarity, identical interaction strengths are not required, and the gate mechanism remains robust against moderate variations in the relative positions of the particles.

Neglecting the much weaker molecule–molecule interaction [42,43], the dynamics are dominated by the molecule–Rydberg-atom dipole–dipole interaction. The corresponding energy-level structure is illustrated in Fig. 1(b). Each molecular control qubit is described by three states $|0\rangle$, $|1\rangle$, and $|2\rangle$, where the transition $|0\rangle \leftrightarrow |2\rangle$ carries a

Received 13 April 2026; accepted 28 July 2026; published 26 August 2026
© 2026 Chinese Physical Society and IOP Publishing Ltd. All rights, including for text and data mining, AI training, and similar technologies, are reserved.

Check for updates

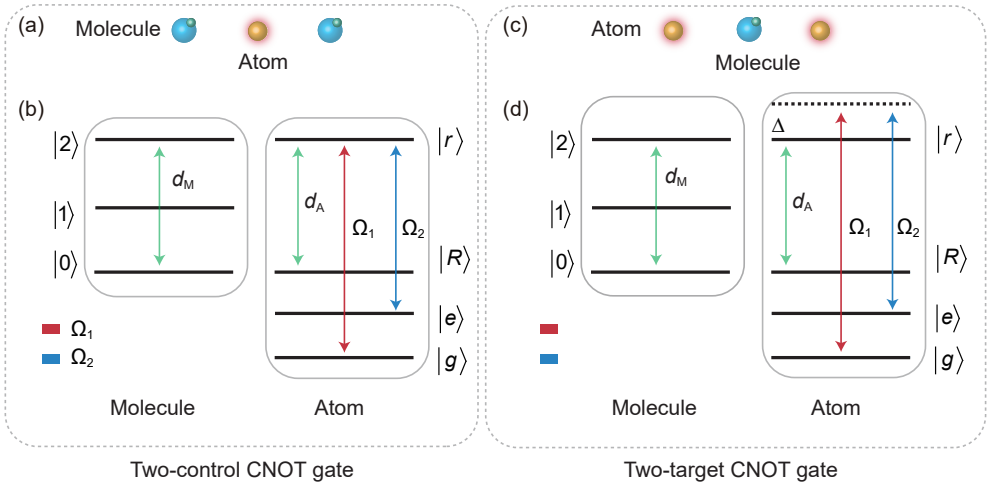

Fig. 1. Hybrid two-control CNOT gate (left) and two-target CNOT gate (right): system configurations and corresponding energy levels. (a) and (b) Two-control CNOT gate. The system consists of one ^{87}Rb atom and two CaF molecules, where the molecules serve as control qubits and the atom acts as the target qubit. (b) shows the corresponding molecule–Rydberg-atom energy levels: the molecule has states $|0\rangle$, $|1\rangle$, and $|2\rangle$, while the atom has ground states $|g\rangle$, $|e\rangle$ and Rydberg states $|R\rangle$, $|r\rangle$. The transitions are driven by laser fields with Rabi frequencies Ω_1 and Ω_2. (c) and (d) Two-target CNOT gate. The system consists of one CaF molecule and two Rydberg atoms. (d) shows the corresponding energy levels: the molecular levels are the same as in (b), while for the atoms the laser fields with Rabi frequencies Ω_1 and Ω_2 couple the ground states to the Rydberg state $|r\rangle$ with a detuning Δ.

dipole moment d_M. In contrast, the atomic target qubit comprises two ground states $|g\rangle$ and $|e\rangle$, together with two Rydberg states $|R\rangle$ and $|r\rangle$, with a dipole moment d_A associated with the transition $|R\rangle \leftrightarrow |r\rangle$. Resonant laser fields couple the Rydberg state $|r\rangle$ to the ground states $|g\rangle$ and $|e\rangle$ with effective Rabi frequencies Ω_1 and Ω_2, respectively. These couplings are realized via two-photon excitation through an off-resonant intermediate state. The associated dynamical AC Stark shifts can be compensated by applying additional far-detuned laser fields, allowing us to employ the effective two-level description used here [see the Supplementary Materials (SM)]. At the same time, by applying an external electric field, the molecular rotational transition $|0\rangle \leftrightarrow |2\rangle$ can be tuned into resonance with the atomic Rydberg transition $|r\rangle \leftrightarrow |R\rangle$, establishing a molecule–Rydberg-atom dipole–dipole interaction mediated by the transition dipole moments d_M and d_A (see the SM for details). The total Hamiltonian of the system can then be written as ($\hbar = 1$)

$$\hat{H}_1 = \frac{\Omega_1}{2}|g\rangle\langle r| + \frac{\Omega_2}{2}|e\rangle\langle r| + \frac{V}{2}\sum_{j=1}^{2}|0\rangle_j\langle 2|\otimes|r\rangle\langle R| + \text{H.c.}, \tag{1}$$

where V denotes the dipole–dipole interaction strength between the molecule and the Rydberg atom, and j labels the two molecular qubits. We consider the subspace spanned by $\{|00g\rangle, |00e\rangle, |10g\rangle, |10e\rangle, |01g\rangle, |01e\rangle, |11g\rangle, |11e\rangle\}$. In the regime $|V| \gg \{|\Omega_1|, |\Omega_2|\}$, when at least one molecule occupies $|0\rangle$ (i.e., in the subspace consisting of $|00\rangle$, $|01\rangle$, and $|10\rangle$), the atomic Rydberg state $|r\rangle$ is resonantly coupled to the molecular auxiliary state via the transition $|0r\rangle \leftrightarrow |2R\rangle$. This strong coupling hybridizes the states into dressed states separated by an energy on the order of V, giving rise to an Autler-Townes splitting [44]. As a result, the excitation is shifted out of resonance, which suppresses laser-driven population transfer to the Rydberg manifold. Consequently, transitions from $|g\rangle$ and $|e\rangle$ to $|r\rangle$ are strongly inhibited, leaving the atomic state unchanged. In contrast, when both molecular qubits occupy $|1\rangle$ (i.e., in the subspace consisting of $|11g\rangle$ and $|11e\rangle$), the molecule–Rydberg-atom interaction vanishes. In practice, the external electric field induces a weak residual off-resonant coupling in this state. However, its strength is approximately four orders of magnitude smaller than that of the resonant interaction V, and it can therefore be safely neglected (see the SM). Consequently, the atomic qubit undergoes a coherent transition between $|g\rangle$ and $|e\rangle$. The corresponding effective Hamiltonian reduces to $\hat{H}_1^{\text{eff}} = \Omega_1/2|11g\rangle\langle 11r| + \Omega_2/2|11e\rangle\langle 11r| + \text{H.c.}$ [45]. By setting $\Omega_1 = -\Omega_2 = \Omega$, the desired hybrid two-control CNOT gate is realized after a gate duration $T = 2\pi/(\sqrt{2}\Omega)$.

We now consider the complementary multi-target scenario, in which a single control qubit simultaneously governs two target qubits, effectively realizing a two-target CNOT gate in a single step. The spatial configuration is shown in Fig. 1(c), where the molecule is located equidistant from the two Rydberg atoms. Each atom is driven by two laser fields with Rabi frequencies Ω_1 and Ω_2, coupling the transitions $|g\rangle \leftrightarrow |r\rangle$ and $|e\rangle \leftrightarrow |r\rangle$, respectively, with a common detuning Δ, as illustrated in Fig. 1(d). The Hamiltonian of the hybrid system is given by

$$\begin{aligned}\hat{H}_2 = \sum_{k=1}^{2}\Big[&\Big(\frac{\Omega_1}{2}|g\rangle_k\langle r| + \frac{\Omega_2}{2}|e\rangle_k\langle r| \\ &+ \frac{V}{2}|0\rangle\langle 2|\otimes|r\rangle_k\langle R|\Big) + \text{H.c.} - \Delta|r\rangle_k\langle r|\Big] \\ &+ U_r|rr\rangle\langle rr| + U_R|RR\rangle\langle RR|,\end{aligned} \tag{2}$$

where U_r and U_R denote van der Waals interaction strengths, and k label the two atomic qubits.

The rapid phase evolution associated with the Rydberg-Rydberg interactions is eliminated by transforming into the rotating frame defined by $U = \exp[-it(U_r|rr\rangle\langle rr| + U_R|RR\rangle\langle RR|)]$, yielding $\hat{H}_2' = U^\dagger\hat{H}_2U + i\dot{U}^\dagger U$. In the strong interactions $\{|U_r|, |U_R|\} \gg \{|\Delta|, |V|, |\Omega_1|, |\Omega_2|\}$, rapidly oscillating terms associated with Rydberg-Rydberg interactions can be neglected. The dynamics are then restricted to the computational subspace spanned by $\{|0gg\rangle, |0ge\rangle, |0eg\rangle, |0ee\rangle, |1gg\rangle, |1ge\rangle, |1eg\rangle, |1ee\rangle\}$. When the molecular control qubit is in state $|0\rangle$, the molecule-Rydberg-atom interaction dominates the dynamics. In the regime $\{|V|, |\Delta|\} \gg \{|\Omega_1|, |\Omega_2|\}$, the intermediate Rydberg-excited states (e.g., $|0gr\rangle$, $|0rg\rangle$, $|0er\rangle$, and $|0re\rangle$) are resonantly coupled to auxiliary states (e.g., $|2gR\rangle$, $|2Rg\rangle$, $|2eR\rangle$, and $|2Re\rangle$), forming dressed states with large energy shifts. As a result, these states are shifted out of resonance with the driving fields, and transitions within this subspace are strongly suppressed. The computational basis states remain unchanged when the molecular qubit is in $|0\rangle$.

When the molecular control qubit occupies the state $|1\rangle$, the molecule–Rydberg-atom interaction is neglected. Under the condition $|\Delta| \gg \{|\Omega_1|, |\Omega_2|\}$, the effective Hamiltonian can be derived to second order in perturbation theory as $\hat{H}_2^{\text{eff}} = \Omega_1\Omega_2/(4\Delta)(|1gg\rangle + |1ee\rangle)(\langle 1ge| + \langle 1eg|) + \text{H.c.} + \Omega_1^2/(4\Delta)(2|1gg\rangle\langle 1gg| + |1ge\rangle\langle 1ge| + |1eg\rangle\langle 1eg|) + \Omega_2^2/(4\Delta)(2|1ee\rangle\langle 1ee| + |1ge\rangle\langle 1ge| + |1eg\rangle\langle 1eg|)$. The dynamics within the ground-state subspace $\{|1gg\rangle, |1ge\rangle, |1eg\rangle, |1ee\rangle\}$ are governed by

effective Raman-type transitions arising from second-order virtual excitations. By applying identical driving fields $\Omega_1 = \Omega_2 = \Omega$, the system undergoes an effective Rabi oscillation after an interaction time $T = 2\pi/(\Omega^2/\Delta)$, implementing the desired hybrid two-target CNOT gate.

Recently, coherence times exceeding 100 ms have been demonstrated for optically trapped CaF molecules [46], which are several orders of magnitude longer than the gate durations considered here. Molecular-qubit decoherence is therefore neglected in the present model. We instead focus on the dominant imperfections associated with the atomic Rydberg qubits, namely Doppler shifts induced by atomic thermal motion, Rydberg-state decay due to spontaneous emission and blackbody-radiation-induced transitions, and off-resonant photon scattering from the intermediate excited state during the two-photon Rydberg excitation. Details of the corresponding estimates are provided in the SM.

To incorporate these effects quantitatively, the atomic qubit is encoded in the two hyperfine ground states $|g\rangle = |5S_{1/2}, F = 1, m_F = 0\rangle$ and $|e\rangle = |5S_{1/2}, F = 2, m_F = 0\rangle$, while the Rydberg states are chosen as $|r\rangle = |59S_{1/2}, m_j = -1/2\rangle$ and $|R\rangle = |58P_{3/2}, m_j = -3/2\rangle$, whose van der Waals dispersion coefficients are $C_6^s/(2\pi) = -115.4$ GHz $(\mu m)^6$ and $C_6^p/(2\pi) = 210.5$ GHz $(\mu m)^6$, respectively, with the latter corresponding to the configuration where the interatomic axis is perpendicular to the quantization axis. At $T = 77$ K, the total decay rates arising from spontaneous emission and black-body-radiation-induced transitions are estimated using the Alkali Rydberg Calculator to be $\gamma_r = 2\pi\times 0.96$ kHz for $|r\rangle$ and $\gamma_R = 2\pi\times 0.60$ kHz for $|R\rangle$ [47]. Additional phase noise is modeled by the dephasing parameter $\gamma_\phi = 2\pi\times 5$ kHz, chosen conservatively to exceed the estimated contribution from off-resonant scattering through the intermediate excited state. The open-system dynamics of the two gate configurations are governed by $\dot{\rho}_i = -i[\hat{H}_i, \rho_i] + \mathcal{L}_i(\rho_i)$, where $i = 1, 2$ denote the hybrid two-control and two-target CNOT gates, respectively. Doppler shifts due to atomic thermal motion are incorporated into $\hat{H}_i$, and the resulting dynamics are averaged over the thermal velocity distribution. The dissipative contribution is written as $\mathcal{L}_i(\rho_i) = \sum_{j,k}(L_j^k \rho_i L_j^{k\dagger} - \{L_j^{k\dagger} L_j^k, \rho_i\}/2)$. Assuming equal branching probabilities from each Rydberg state to the two computational states, the decay operators for the jth atom are $L_j^0 = \sqrt{\gamma_r/2}|g\rangle_j\langle r|$, $L_j^1 = \sqrt{\gamma_r/2}|e\rangle_j\langle r|$, $L_j^2 = \sqrt{\gamma_R/2}|g\rangle_j\langle R|$, and $L_j^3 = \sqrt{\gamma_R/2}|e\rangle_j\langle R|$. Rydberg-state dephasing is described by $L_j^4 = \sqrt{\gamma_\phi}|r\rangle_j\langle r|$ and $L_j^5 = \sqrt{\gamma_\phi}|R\rangle_j\langle R|$.

Figure 2 shows the fidelity evolution of the hybrid two-control and two-target CNOT gates. The fidelity is defined as $F = \langle\Psi_{\text{ideal}}|\rho(t)|\Psi_{\text{ideal}}\rangle$, where $\rho(t)$ is the system density matrix and $|\Psi_{\text{ideal}}\rangle$ is the corresponding ideal output state. To improve robustness against control imperfections, we employ a time-dependent Gaussian pulse $\Omega(t) = \Omega_{\max}\exp[-(t-t_0)^2/(2\sigma^2)]$, where $\Omega_{\max}$, t_0, and σ denote the peak amplitude, pulse center, and pulse width, respectively. The smooth pulse profile suppresses nonadiabatic switching effects and unwanted off-resonant excitation. For both gate configurations, the molecule–Rydberg-atom interaction strength is fixed at $V = 2\pi\times 4.04$ MHz.

For the two-control CNOT gate, the operation time T is determined by the pulse-area condition $\int_0^T \sqrt{2}\Omega(t)dt = 2\pi$. The pulse parameters are chosen as $\Omega_{\max} = 2\pi\times 1.05$ MHz, $t_0 = T/2$, and $\sigma = 0.27$ μs. We take the initial state to be $|\Psi\rangle = (1/2)\sum_{i,j=0}^{1}|ij\rangle\otimes|-\rangle_A$, where $|-\rangle_A = (|g\rangle - |e\rangle)/\sqrt{2}$. The corresponding ideal output state is $|\Psi_{\text{ideal}}\rangle = (1/2)(|00\rangle + |01\rangle + |10\rangle - |11\rangle)\otimes|-\rangle_A$. The relative minus sign of the $|11\rangle$ component arises because the target qubit is flipped only when both control qubits occupy the logical state $|1\rangle$.

For the two-target CNOT gate, the effective second-order coupling imposes the pulse-area condition $\int_0^T \Omega^2(t)/\Delta dt = 2\pi$. The parameters are chosen as $\Omega_{\max} = 2\pi\times 0.71$ MHz, $t_0 = T/2$, $\sigma = 2.25$ μs, and $\Delta = 2\pi\times 2$ MHz. The Rydberg-Rydberg interaction strengths are $U_r = 2\pi\times 1789.1$ MHz and $U_R = -2\pi\times 3295.3$ MHz. The initial state is $|\Psi'\rangle = |+\rangle_M\otimes|-\rangle_A\otimes|+\rangle_A$, and the corresponding ideal output state is $|\Psi'_{\text{ideal}}\rangle = |-\rangle_M\otimes|-\rangle_A\otimes|+\rangle_A$. Here, $|\pm\rangle_A = (|g\rangle \pm |e\rangle)/\sqrt{2}$ and $|\pm\rangle_M = (|0\rangle \pm |1\rangle)/\sqrt{2}$ denote the atomic and molecular superposition states, respectively.

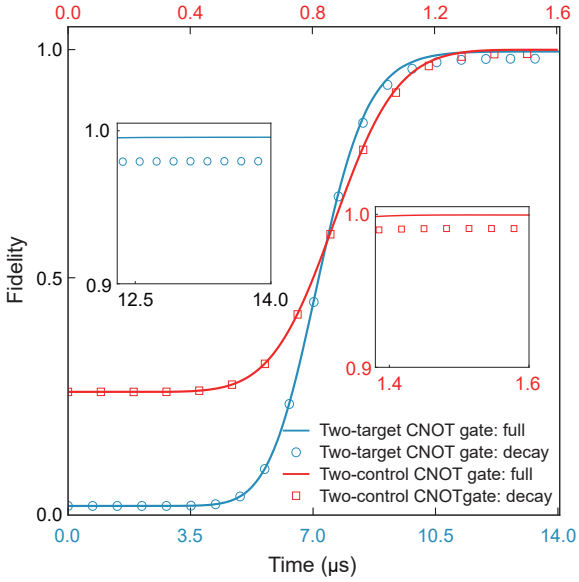

Fig. 2. Time evolution of the gate fidelity obtained from the master equation. Solid lines (open symbols) denote the coherent (dissipative) dynamics. Blue and red correspond to the two-target and two-control CNOT gates, respectively. Both configurations operate with a shared molecule–Rydberg-atom interaction $V = 2\pi\times 4.04$ MHz. For the two-control (two-target) CNOT gate, the pulse parameters are $\Omega_{\max} = 2\pi\times 1.05$ MHz ($2\pi\times 0.71$ MHz), $t_0 = T/2$, and $\sigma = 0.27$ μs (2.25 μs). Insets show enlarged views in the high-fidelity regime. The interaction strengths are $U_r = 2\pi\times 1789.1$ MHz and $U_R = -2\pi\times 3295.3$ MHz. The detuning is $\Delta = 2\pi\times 2$ MHz.

Solid lines, shown in red for the two-control gate and blue for the two-target gate, represent the ideal dynamics generated by the full Hamiltonians $\hat{H}_1$ in Eq. (1) and $\hat{H}_2$ in Eq. (2), respectively, while open symbols denote the corresponding dissipative dynamics obtained from the master equation. As shown in the insets, the relevant decoherence causes only a moderate reduction in the gate fidelity. The dissipative dynamics remain close to the ideal evolution, and both gates retain high final fidelities, demonstrating the robustness of the proposed scheme under realistic conditions.

Although a native single-pulse two-target CNOT gate often requires a longer operation time than a standard two-control CNOT gate, exploring its implementation is highly necessary. In practical quantum control, the overall fidelity is limited not only by decoherence but also heavily by control errors, crosstalk, and state leakage. By replacing a deep cascade of CNOTs with a single, carefully shaped driving field, we trade an increase in decoherence time for a reduction in pulse-edge errors and algorithmic circuit depth. This holistic error mitigation makes such long-duration multi-target gates particularly valuable for efficient circuit compilation and robust quantum error correction.

Finally, the scalability of the proposal is demonstrated by extending the schemes to four-qubit implementations, namely three-control and three-target CNOT gates. For the three-control CNOT gate, the system is expanded by introducing an additional molecule, as shown in the top inset of Fig. 3, where three molecules are arranged at the vertices of an equilateral triangle and the target Rydberg atom is located at the centroid, such that molecule–molecule interactions remain negligible. For the three-target CNOT gate, an additional Rydberg atom is incorporated into the target array, as illustrated in the bottom inset of Fig. 3. In both configurations, fidelity increases smoothly during gate operation and saturates above 99%. These results demonstrate that the proposed four-qubit CNOT gates can be implemented with high fidelity, highlighting the potential of this hybrid platform for scaling to larger quantum systems (see the SM for details).

In conclusion, we have proposed and numerically investigated a

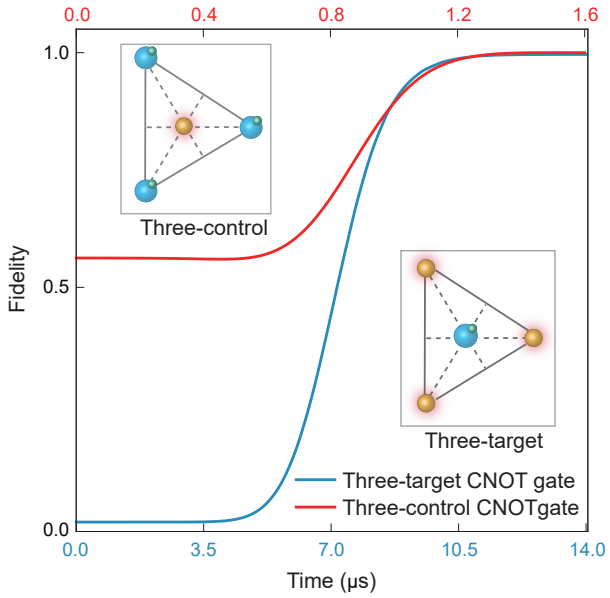

Fig. 3. Fidelity evolution for the three-control (red curve, top axis) and three-target (blue curve, bottom axis) configurations. Insets depict the corresponding spatial arrangements. Parameters are the same as those in Fig. 2, except that, for the three-target CNOT gate, the Rydberg-Rydberg interaction strengths are set to $U_r = 2\pi \times 4240.7$ MHz and $U_R = -2\pi \times 7796$ MHz. The molecule–Rydberg-atom interaction strengths are given in the SM.

scheme for implementing multipartite CNOT gates in a hybrid molecule-Rydberg-atom system. By combining the long coherence times of molecular ground states with the strong and tunable interactions enabled by Rydberg excitations, the scheme realizes both two-control and two-target CNOT gates within a unified framework. We have further examined the effects of realistic imperfections, including Doppler shifts induced by atomic thermal motion, off-resonant photon scattering from the intermediate state, and Rydberg-state decay due to spontaneous emission and black-body-radiation-induced transitions. These decoherence mechanisms do not qualitatively alter the operating principle of the gates, and high fidelities can still be maintained under experimentally relevant conditions. Moreover, the direct realization of multipartite gates in a single step can reduce the circuit depth relative to conventional decompositions into sequences of two-qubit gates. The scalability of the scheme is further demonstrated by extending the protocol to three-control and three-target CNOT gates, indicating that the same interaction mechanism can be naturally generalized to larger multipartite systems. Our results therefore establish hybrid molecule–Rydberg-atom platforms as a promising architecture for efficient multipartite quantum gates and scalable quantum information processing.

Acknowledgements

This work was supported by the National Natural Science Foundation of China (Grant No. 12174048). W. L. acknowledges support from the EPSRC (Grant No. EP/W015641/1) and the Going Global Partnerships Programme of the British Council (Contract No. IND/CONT/G/22-23/26).

References

[1] Nielsen M A and Chuang I L 2010 *Quantum Computation and Quantum Information* (Cambridge: Cambridge University Press)
[2] Grover L K 1997 *Phys. Rev. Lett.* **79** 325
[3] Hofmann H F 2005 *Phys. Rev. A* **72** 022329
[4] Paredes B, Verstraete F, and Cirac J I 2005 *Phys. Rev. Lett.* **95** 140501
[5] DiVincenzo D P 1995 *Phys. Rev. A* **51** 1015
[6] Barenco A, Bennett C H, Cleve R, DiVincenzo D P, Margolus N, Shor P, Sleator T, Smolin J A, and Weinfurter H 1995 *Phys. Rev. A* **52** 3457
[7] Üstün G, Morello A, and Devitt S 2024 *Quantum Sci. Technol.* **9** 035037
[8] Graham T M, Song Y Q, Scott J, Poole C, Phuttitarn L, Jooya K, Eichler P, Jiang X, Mariappa A, Greeson J C, Hogan J J, Day T G, Robertson S T, and Saffman M 2022 *Nature* **604** 457
[9] Levine H, Keesling A, Omran A, Bernien H, Schwartz S, Zibrov A S, Endres M, and Lukin M D 2019 *Phys. Rev. Lett.* **123** 170503
[10] Takeda K, Noiri A, Nakajima T, Kobayashi T, and Tarucha S 2022 *Nature* **608** 682
[11] Zhou Y N, He H, Pang F, Lyu H, Zhang Y J, and Chen X 2025 *Phys. Rev. A* **111** 042616
[12] Sun Y, Xu P, Chen P X, and Liu L 2020 *Phys. Rev. Appl.* **13** 024059
[13] Yang C P, Su Q P, Zhang Y, and Nori F 2020 *Phys. Rev. A* **101** 032329
[14] Xiang Z L, Ashhab S, You J Q, and Nori F 2013 *Rev. Mod. Phys.* **85** 623
[15] Kurizki G, Bertet P, Kubo Y, Mølmer K, Petrosyan D, Rabl P, and Schmiedmayer J 2015 *Proc. Natl. Acad. Sci. USA* **112** 3866
[16] Shao X Q, Su S L, Li L, Nath R, Wu J H, and Li W B 2024 *Appl. Phys. Rev.* **11** 031320
[17] Tomza M, Jachymski K, Gerritsma R, Negretti A, Calarco T, Idziaszek Z, and Julienne P S 2019 *Rev. Mod. Phys.* **91** 035001
[18] Langenfeld S, Welte S, Hartung L, Daiss S, Thomas P, Morin O, Distante E, and Rempe G 2021 *Phys. Rev. Lett.* **126** 130502
[19] Reiserer A, Kalb N, Rempe G, and Ritter S 2014 *Nature* **508** 237
[20] Reiserer A, Ritter S, and Rempe G 2013 *Science* **342** 1349
[21] Zhang C, Pokorny F, Li W B, Higgins G, Pöschl A, Lesanovsky I, and Hennrich M 2020 *Nature* **580** 345
[22] Su S L, Wang C, Song P Y, and Chen G 2024 *Chin. Phys. Lett.* **41** 040302
[23] Bluvstein D, Evered S J, Samutpraphoot P *et al* 2024 *Nature* **626** 58
[24] Barredo D, de Léséleuc S, Lienhard V, Lahaye T, and Browaeys A 2016 *Science* **354** 1021
[25] Li S Z, Zhang Y C, Wang Y, Zhang S, Zhu S L, and Li Z 2026 *Sci. China-Phys. Mech. Astron.* **69** 217212
[26] Beterov I I, Ryabtsev I I, Tretyakov D B, and Entin V M 2009 *Phys. Rev. A* **79** 052504
[27] Browaeys A, Barredo D, and Lahaye T 2016 *J. Phys. B: At. Mol. Opt. Phys.* **49** 152001
[28] Saffman M 2016 *J. Phys. B: At. Mol. Opt. Phys.* **49** 202001
[29] Li B B, Zhao Y, Xu S L, Zhou Q, Fu Q D, Ye F W, Hua C B, Chen M W, Hu H J, Zhou Q Q, and Qiu Z C 2023 *Chin. Phys. Lett.* **40** 044201
[30] Hu Y D, Zhang Y C, Jie Q X, Fan H J, Zhong X K, Ma D Q, Lv Y N, Zhang Y L, Zou X B, Kang S B, Guo G C, Wang Z B, and Zou C L 2026 *Chin. Phys. Lett.* **43** 040303
[31] Farouk M, Beterov I I, Xu P, Bergamini S, and Ryabtsev I I 2023 *Photonics* **10** 1280
[32] Zeng Y, Xu P, He X, Liu Y, Liu M, Wang J, Papoular D J, Shlyapnikov G V, and Zhan M 2017 *Phys. Rev. Lett.* **119** 160502
[33] Dobrzyniecki J and Tomza M 2023 *Phys. Rev. A* **108** 052618
[34] Sawant R, Blackmore J A, Gregory P D, Mur-Petit J, Jaksch D, Aldegunde J, Hutson J M, Tarbutt M R, and Cornish S L 2020 *New J. Phys.* **22** 013027
[35] Gregory P D, Blackmore J A, Bromley S L, Hutson J M, and Cornish S L 2021 *Nat. Phys.* **17** 1149
[36] Yan B, Moses S A, Gadway B, Covey J P, Hazzard K R A, Rey A M, Jin D S, and Ye J 2013 *Nature* **501** 521
[37] Tobias W G, Matsuda K, Li J R, Miller C, Carroll A N, Bilitewski T, Rey A M, and Ye J 2022 *Science* **375** 1299
[38] Wang K, Williams C P, Picard L R B, Yao N Y, and Ni K K 2022 *PRX Quantum* **3** 030339
[39] Zhang C and Tarbutt M R 2022 *PRX Quantum* **3** 030340
[40] Zhang C, Murciano S, Tantivasadakarn N, and Finkelstein R 2026 arXiv:2602.12909 [quant-ph]
[41] Zhu L, Luke J, Shaham R, Liu Y X, and Ni K K 2025 *Phys. Rev. Lett.* **135** 153001
[42] Guttridge A, Ruttley D K, Baldock A C, González-Férez R, Sadeghpour H R, Adams C S, and Cornish S L 2023 *Phys. Rev. Lett.* **131** 013401
[43] Guttridge A, Hepworth T R, Ruttley D K, Durst A A T, Eiles M T, and Cornish S L 2025 *Phys. Rev. Lett.* **134** 133401
[44] Autler S H and Townes C H 1955 *Phys. Rev.* **100** 703
[45] Brion E, Pedersen L H, Mølmer K, Chutia S, and Saffman M 2007 *Phys. Rev. A* **75** 032328
[46] Burchesky S, Anderegg L, Bao Y, Yu S S, Chae E, Ketterle W, Ni K K, and Doyle J M 2021 *Phys. Rev. Lett.* **127** 123202
[47] Robertson E J, Šibalić N, Potvliege R M, and Jones M P A 2021 *Comput. Phys. Commun.* **261** 107814